Research paper

Using Small-Footprint and Multiple-Return LiDAR Data to Characterize and Classify Four Temperate Forest Cover Types

Yi-Ta Hsieh,[1] Chaur-Tzuhn Chen,[2] Shou-Tsung Wu[3,4]

【Summary】

The information of the foliage cover and the distribution of branches are essential sources for understanding the spatial variability of the vertical forest structure. But it is difficult to use traditional research methods, such as doing field surveys and interpreting aerial photographs, to obtain related information on the vertical forest structure and conditions below the canopy. Therefore, this study attempted to evaluate the possibilities of using airborne LiDAR data to examine the forest vertical structure below the canopy, and utilize LiDAR data to classify land cover types in mountain areas. Red cypress (*Chamaecyparis formosensis*), Sugi (*Cryptomeria japonica*), mixed hardwoods, and bare land were the 4 categories analyzed in the investigated area, the Alishan region of central Taiwan. The analytical methods were based on LiDAR multiple-return and intensity data, and statistical analyses and image classification were used to describe the diversities of the investigated land types. The ratio of echo model (REM) and echo intensity model (EIM) were effective in distinguishing the divergences of different land types. Results of this study demonstrated the proportion of echo return and intensity data related to the canopy density. Among the types of test echoes used in the study, plentiful information for land cover classification using both the ratio of echo returns and the intensity of echoes was acquired from the first echo returns. The results of applying single-image classification showed a classification accuracy of 50.5~68.5%. The EIM_{FE}, REM_{FE}, REM_{LE}, and REM_{OE} showed a higher potential for classifying land types. The classification results of stack images indicated that combining more LiDAR-derived variables yielded a more-accurate classification accuracy (81.5%). This study corroborates the high feasibility for mapping land cover types using LiDAR multiple-return and intensity data.

Key words: LiDAR, multiple-return, intensity, classification.

Hsieh YT, Chen CZ, Wu ST. 2014. Using small-footprint and multiple-return LiDAR data to characterize and classify four temperate forest cover types. Taiwan J For Sci 29(1):53-68.

[1] Graduate of Bioresources, National Pingtung Univ. of Science and Technology, 1 Xuefu Rd., Neipu Township, Pingtung 91201, Taiwan. 國立屏東科技大學生物資源研究所，91201屏東縣內埔鄉學府路1號。

[2] Department of Forestry, National Pingtung Univ. of Science and Technology, 1 Xuefu Rd., Neipu Township, Pingtung 91201, Taiwan. 國立屏東科技大學森林系，91201屏東縣內埔鄉學府路1號。

[3] Department of Tourism Management, Shih Chien Univ. 200 Univ. Rd., Neimen Township, Kaohsiung 84550, Taiwan. 實踐大學高雄校區觀光管理學系，84550高雄縣內門鄉大學路200號。

[4] Corresponding author, e-mail:st.wu@msa.hinet.net 通訊作者。

Received May 2013, Accepted December 2013. 2013年5月送審 2013年12月通過。

研究報告

小覆蓋面多重回波光達資料應用於四個溫帶森林覆蓋類型之特徵與分類探討

謝依達[1)] 陳朝圳[2)] 吳守從[3,4)]

摘 要

樹葉覆蓋與枝條分佈的資訊為理解森林垂直結構空間變異的基本要素，然而透過傳統的田野調查研究或航空照片判釋，卻很難有效獲取森林垂直結構與冠層以下的相關資訊；因此，本研究旨在評估利用空載光達資料探討冠層下森林垂直結構的可行性，並進行山區森林植群分類。本研究以阿里山地區為範圍，其內計有紅檜(*Chamaecyparis formosensis*)、柳杉(*Cryptomeria japonica*)、闊葉樹混淆林與裸露地等四種類型，因此透過空載光達多重回波與強度值資料，結合統計分析與影像分類探討其差異性。研究指出，回波比率模型(REM)與回波強度模型(EIM)能有效區分土地利用類型的不同，同時證明回波比率與強度和林分冠層密度具有相關性，其中第一回波的回波比率與強度值最能充分反應冠層資訊。至於影像分類方面，單一影像的分類準確度介於50.5至68.5%之間，且第一回波強度(EIM_{FE})、第一回波比率(REM_{FE})、最終回波比率(REM_{LE})與單一回波比率(REM_{OE})具有較高的分類潛力；不過融合較多變數的混合影像，其分類準確度更高，達81.5%。因此本研究證實，透過空載光達的多重回波與強度值資料，確可有效進行土地覆蓋類型的分類與製圖工作。

關鍵詞：空載光達、多重回波、強度值、分類。

謝依達、陳朝圳、吳守從。2014。小覆蓋面多重回波光達資料應用於四個溫帶森林覆蓋類型之特徵與分類探討。台灣林業科學29(1):53-68。

INTRODUCTION

The information embedded in the foliage cover and the distribution of branches are essential sources for understanding the spatial variability of the vertical forest structure. Various tree species and forest types lead to complicated and diverse vertical characteristics of forest structure, and it is difficult to apply traditional research methods, such as doing field surveys and interpreting aerial photographs, to obtain related information on the vertical forest structure and conditions below the canopy. Fortunately over the past decade, remote sensing techniques, such as LiDAR, have rapidly become popularly used as tools for extracting 3-dimensional (3D) forest information.

Airborne laser scanning (ALS), also termed airborne LiDAR (light detection and ranging), is one of many laser remote-sensing techniques (Raymond 1992) that direct a near infrared laser pulse downwards towards the earth's surface (Lefsky et al. 2002), and measure the return time of each beam traveling between the sensor and a target using ultra-accurate clocks (Suarez et al. 2005). LiDAR can provide 3D information for the highly automated generation of digital elevation models (DEMs), and some studies also showed the potential of LiDAR data to derive forest variables (such as stand height,

basal area, stem volume, and biomass) (Nilsson 1996, Næsset 1997a, b, 2002, Lefsky et al. 1999, Means et al. 2000, Zimble et al. 2003, Maltamo et al. 2004). In fact, LiDAR-measured forest structural attributes were often based on a LiDAR-derived canopy height model (CHM) with ground survey data using a regression analysis (e.g., k-MSN regression, SVM-regression, or k-NN classification) to build regression models.

The small-footprint LiDAR emits a small beam of light, and most small-footprint LiDAR systems have the feature of multiple-return that is capable of recording the discrete return (the laser pulse return also referred to as the "echo"). The characteristic of multiple-returns often occurs in forest land, because the emitted laser light can pass through vegetation, and it carries a lot of information about the forest's internal structures. The distribution of laser echoes in a tree is the result of the canopy density, tree shape, and foliage distribution (Ørka et al. 2007). Some studies applied the LiDAR multiple-return character to obtain important information on the vegetation density and structure. Morsdorf et al. (2006) estimated the leaf area index (LAI) according to the first, last, and only echo data of LiDAR. Holmgren and Persson (2004) identified individual tree species by analyzing the proportion of returning data that contained the ratio of only returns and the ratio of first returns. Donoghue et al. (2007) used the proportion of ground return data to classify tree species. Takahashi et al. (2006) demonstrated that the rate of LiDAR-derived laser penetration, calculated by multiple-return characters, between Hinoki cypress (*Chamaecyparis obtusa*) and Sugi (*Cryptomeria japonica*) stands significantly differed. Different forest types would lead different laser penetrations, which may be caused by different leaf branches, tree shapes, and canopy densities. Using those characters can help classify different forest types. Many novel systems of small-footprint LiDAR can also obtain data on the intensity of each return, which is defined as the ratio of the strength of the reflected light. The LiDAR intensity is influenced by the reflectance of the reflecting object and materials with different reflectance properties (Song et al. 2002). The intensity of the return (which has no units) provides useful information on the characteristics of pseudo near-infrared reflectance from objects (Wehr and Lohr 1999). Early on, Schreier et al. (1985) found that the LiDAR intensity afforded information of vegetation density and vegetation type, and the mean intensity and intensity variability measured by LiDAR systems could be used to identify coniferous and deciduous trees. In recent years, quite a few researchers have employed intensity data to identify tree species (Holmgren and Persson 2004, Moffiet et al. 2005, Donoghue et al. 2007, Ørka et al. 2007), classify urban land-use (Song et al. 2002, Bartels and Wei 2006), and recognize glacier surfaces (Höfle et al. 2007). Donoghue et al. (2007) used the different intensity data on the 25^{th}, 50^{th}, 75^{th} and 90^{th} tree height percentiles to identify tree species mixtures in conifer plantations. Donoghue et al. (2007) also noted that higher-intensity percentiles provided a measure of reflectivity of the forest canopy, while lower-intensity percentiles provided a measure of woody material. Ørka et al. (2007) used the intensity of the mean and standard deviation among first, last, and only echo data for tree species classification.

This study focuses on describing forest structures in different forest types using LiDAR multiple-return and intensity data. We employed the intensity data and return proportions from different echo types, and different echo types were reflected within different tree layers. For this reason, the echo intensity

and return proportion were expected to provide higher variability among forest types.

MATERIALS AND METHODS

Study area

The investigated area of this study was located within the Alishan National Scenic Area, the most popular tourist resort in central Taiwan (Fig. 1). It covers 788.4 ha, and its landscape is characterized as alpine terrain. The elevation within this investigated area ranges 1438~2421 m. The most common forest types in this area are *Chamaecyparis formosensis* (red cypress), *Cryptomeria japonica* (Sugi) stand plantations, and natural forests of mixed hardwoods.

LiDAR data

The airborne LiDAR data used in this research were collected from flights organized by the Industrial Technology Research Institute (Hsinchu, Taiwan). LiDAR data were acquired in June 2006 using the Leica ALS50 system (Leica, Wetzlar, Germany), operated from an airplane at a flight altitude of 3000 m above sea level with an average speed of 110 knots, and with a point density of 2~4 points m^{-2}. There were 10 east-west flight lines covering the surveyed area, and adjacent flight lines had a side-overlap of approximately 40%. The field of view (FOV) was 50˚ for the LiDAR data. Four types of return point cloud data (first, second, last, and only echoes) were recorded by the Leica ALS50 system (Table 1). Like most discrete return data of LiDAR systems, the Leica ALS50 also records the intensity of each pulse in the near infrared at a1064-nm wavelength.

Reference data

Aerial photographs

Aerial photographs were simultaneously collected together with LiDAR data using

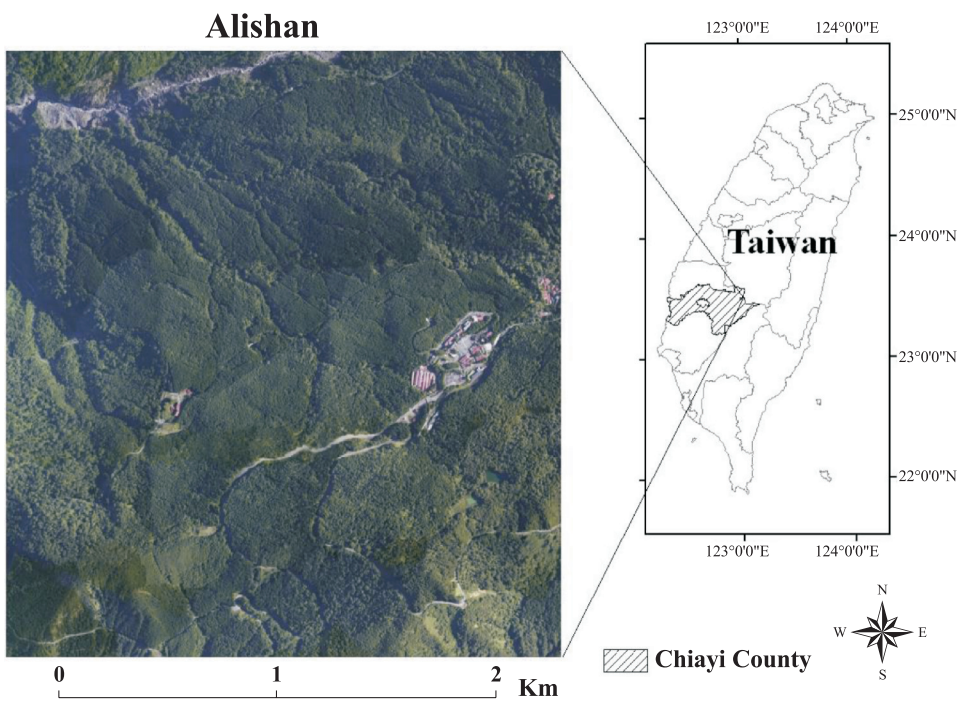

Fig. 1. Aerial photograph of the investigated area (in central Taiwan) for this study.

Table 1. Definitions of echo types

Echo type	Definition
First echo	First return of multiple-returns
Second echo	Second return of multiple-returns
Last echo	Last return of multiple-returns
Only echo	Single return

a Leica ADS40 airborne digital sensor. The aerial photographs were used to validate the forest species composition and had a spatial resolution of 0.5 m.

Land use map

A land-use map was also utilized in this study as an auxiliary tool to help interpret the aerial photos. The land-use map was part of the *Third Forest Resources and Land Use Inventory in Taiwan* (by the Forestry Bureau, Taipei, Taiwan). However, this map was sketched in 1989~1993, and some changes in land cover could have occurred since then.

Methods

Definition of forest types

Before analyzing the LiDAR variables for each forest type, it was necessary to recognize the main forest types in the research area to facilitate further data extraction and analysis. Four major land types were recognized in the area according to the land-use map and through interpretation of aerial photographs: red cypress (*Chamaecyparis formosensis*), sugi (*Cry. japonica*), mixed hardwoods (*Neolitsea acuminatissma*, *Trochodendron aralioides*, *Illicium tashiroi*, etc.), and bare land. The standard of interpreting samples, outlined as optical differences in land types, is demonstrated in Fig. 2, with views at a scale 1: 1000. The definition of the crown typology for analyzing aerial photos is also indicated in Table 2.

Side views of laser-point distributions with a 10-m depth for each land type are shown on the right side of Fig. 2, and the point clouds were colored by echo types. Distributions of laser points greatly differed according to land types and tree shapes (Fig. 2b, d, f). The laser points showed a higher ratio of the only echo in Sugi than in red cypress and mixed hardwoods. Otherwise, mixed hardwoods had a higher ratio of the multiple return. Bare land just had the only echo (Fig. 2h).

LiDAR data pre-processing

One of the objectives of this study was to classify forest types using LiDAR data, so the first step was to remove unreasonable points from the LiDAR data using Terra-Scan software (Terrasolid). Unreasonable points included those that were too low or too high, so nominal land surface and cloud data points were excluded.

Information from laser points included x, y, and z coordinates, intensity, and echo-type data. The echo type was analyzed in this study for forest type classification.

Derivation of LiDAR variables

Two kinds of datasets were used to analyze the different forest types: the ratio of echo model (REM) and echo intensity model (EIM).

REM

The REM in this study is defined as the percentage of each LiDAR hit of echo types compared to the total LiDAR hits. According to Peng et al. (2008) and the mosaic of vegetation types, the REM was extracted at a 20-m resolution. Ratios of the first, second, last, and only echo numbers were calculated, and ratios of echo types were computed according to Eq. (1) (Moffiet et al. 2005), and its output is illustrated in Fig. 3:

$$REM_{FE,\,SE,\,LE,\,OE} = \frac{N_{FE,\,SE,\,LE,\,OE}}{N_{All}} \quad (1)$$

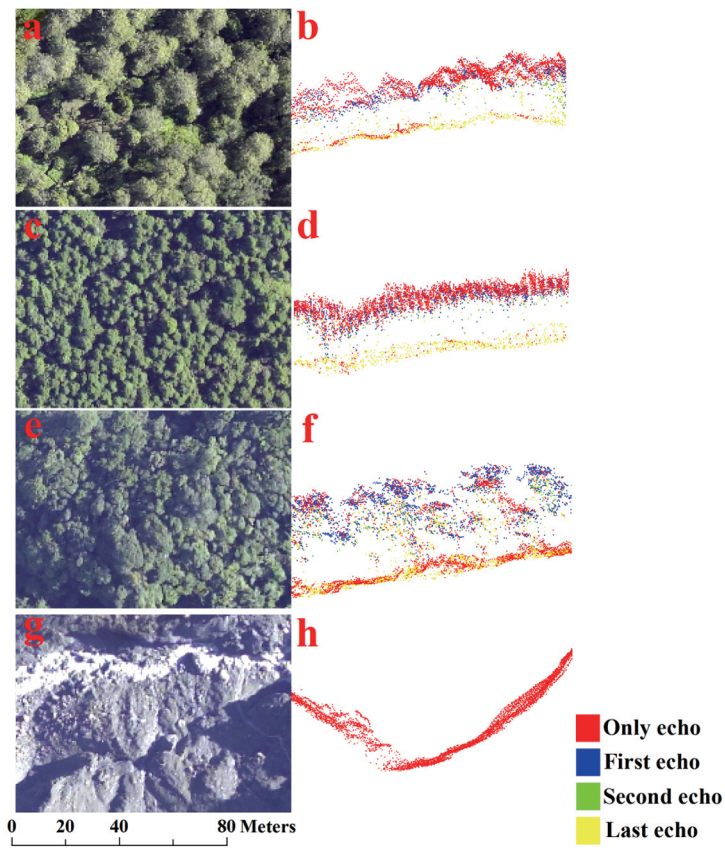

Fig. 2. Four forest cover types in the study area. Aerial photographs of each land type at a scale of 1: 1000 (left), side views of distributions of laser points with a 10-m depth for each land type (right). (a) and (b), red cypress; (c) and (d), Sugi; (e) and (f), mixed hardwoods; (g) and (h), bare land.

Table 2. Definitions of crown typology for interpreting aerial photos

Land cover type	Definition
Red cypress	Larger tree crown size, round crown contour, and rounded curvature of the crown surface
Sugi	Smaller tree crown size, and dotted regular distribution
Mixed hardwoods	Contained many kinds of tree species, large tree crown sizes, and crown contours generally irregular
Bare land	Non-forest land type that contained buildings, roads, riverbeds, and landslide areas

Where REM is the ratio of echo model, N is the number of echo hits, and the subscripts $_{FE,\ SE,\ LE,\ OE,\ and\ All}$ denote the first echo, second echo, last echo, only echo, and all echo, respectively.

EIM

The EIM indicates the LiDAR intensity data for each echo type, and is constructed using the average value of the LiDAR hit intensity at a 20-m resolution (Peng et al.

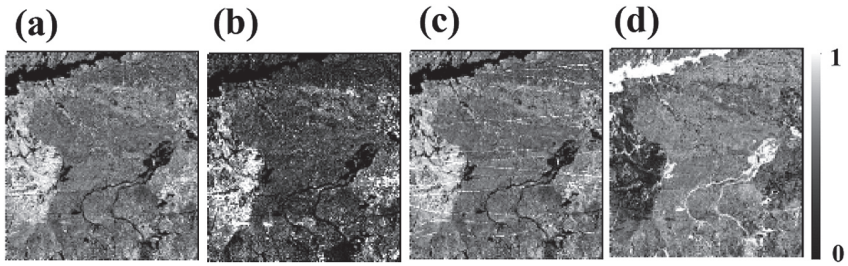

Fig. 3. Ratio of echo model (REM). (a) REM_{FE}, ratio of first echo model; (b) REM_{SE}, ratio of second echo model; (c) REM_{LE}, ratio of last echo model; (d) REM_{OE}, ratio of only echo model.

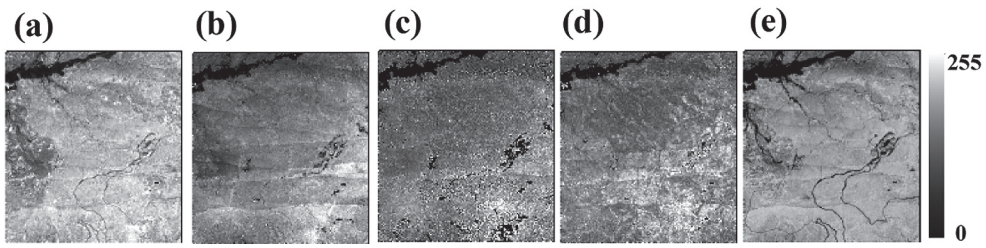

Fig. 4. Echo intensity model (EIM). (a) EIM_{All}, all echo intensity model; (b) EIM_{LE}, last echo intensity model; (c) EIM_{SE}, second echo intensity model; (d) EIM_{FE}, first echo intensity model; (e) EIM_{OE}, only echo intensity model.

2008). The mean intensities of the first, second, last, and only echoes within a pixel were used in this study. The ratio of echo type was computed according to Eq. (2) (Moffiet et al. 2005), and its output is illustrated in Fig. 4:

$$EIM_{FE,\,SE,\,LE,\,OE,\,All} = \frac{\sum I_{FE,\,SE,\,LE,\,OE,\,All}}{N_{All}} \qquad (2)$$

Where EIM is the echo intensity model (it is the average value of intensity in each raster), and the symbol I is the intensity value.

According to Peng et al. (2008), the 20-m spatial resolution was considered to represent more-complete stand characteristics. All of these data above were converted into a raster format with the same 20×20-m cell size. This research recognized the density of the laser point (2.62 points m^{-2}) from this LiDAR data. On average, there were 1048 LiDAR points for each 20×20-m cell; therefore, a suitable resolution was obtained.

Training data evaluation

In order to compare how variables responded among the 4 land cover types, training data were selected by interpreting aerial photographs and the land-use map for each land type (the standard of interpreting data is demonstrated in Table 2). Training data (43 training polygons) were used to analyze each variable in this study (Table 3).

First of all, the transformed divergence (TD) was used to analyze the separability of

Table 3. Numbers of training samples for each type

Land cover type	No. of training samples (no. of pixels)
Red cypress	10 (101)
Sugi	13 (250)
Mixed hardwoods	10 (181)
Bare land	10 (112)

the training data (Eq. 3), and the scale of TD values can range 0~2000. If the result is > 1900, then the classes can be separated. Between 1700 and 1900, the separation is fairly good. Below 1700, the separation is poor (Jensen 1996).

$$D_{ij} = \frac{1}{2} tr\,[(c_i - c_j)(c_i^{-1} - c_j^{-1})] + \frac{1}{2} tr\,[(c_i^{-1} - c_j^{-1})(u_i - u_j)(u_i - u_j)^T]$$

$$TD_{ij} = 2000\left[1 - \exp\left(\frac{-D_{ij}}{8}\right)\right] \quad (3)$$

Where i and j are the 2 signatures (classes) being compared, C_i is the covariance matrix of signature i, μ_i is the mean vector of signature i, tr is the trace function, and T is the transposition function.

A one-way analysis of variance (ANOVA) was also used to analyze the training data of the REM and EIM. The test hypotheses were: H_0 (there was no difference in those variables among the 4 land types) and H_1 (there were differences in those variables among the 4 land types). The significance level was set to 5%. In order to test the significance of each land cover type, Duncan's multiple-range test of significance and correlation was calculated in a post-hoc analysis. The results are useful in determining which variable provides better separability of forest structure and forest types.

LiDAR image classification

Two kinds of data formats were used in this study for further classifications.

Single image: There were 9 LiDAR variable images (4 REM images and 5 EIM images) that were separately used for further classification. The aim of this process was to compare the classification accuracy between these LiDAR variables and understand the most important factor in those variables for land type classification.

Stack image: Stack images were used to collect REM and EIM images, and produced a 9-band stacked image. The aim of this process was to test this fusion approach by mixing all of the variables to obtain more-complete information for classification.

LiDAR single images and stack images were then classified using a supervised classification approach: maximum likelihood classifier (MLC). All processes of classification were carried out using the same training data (Table 3) in order to lead to more-impartial results of classification for comparison with each other. Image processing was carried out using ERDAS IMAGINE 9.1 software (ERDAS).

Accuracy and field validation of the assessment

After classifying the images, the researchers assessed the accuracy of the classification. Because the aerial photographs were taken together with the LiDAR data, there was no time to delay between the 2 data. In the study, 200 check points were selected at random and interpreted using aerial photographs, and uncertain sample points were inventoried by field validation in winter 2007. Then the samples points were used to calculate an error matrix. In addition, the overall accuracy of classification, and the producer's and user's accuracies were also determined through Kappa statistics.

RESULTS AND DISCUSSION

Descriptions of LiDAR variables among different land cover types

The description from the REM

Among 3 classes of forest types from the REM, the REM_{FE}, REM_{SE}, and REM_{LE} showed higher mean values of fraction in red cypress (0.224, 0.042, and 0.229) and mixed hardwoods (0.245, 0.038, and 0.245) than in Sugi (0.168, 0.022, and 0.172, respectively). How-

ever, the REM_{OE} showed a higher mean value of fraction in Sugi (0.639) than in red cypress (0.506) and mixed hardwoods (0.473) (Table 4). This outcome indicates that Sugi yielded a lower percentage of multiple-returns than red cypress and mixed hardwoods, and Sugi provided a higher percentage of single returns. It demonstrates that the permeability of the canopy cover of Sugi is low. Hence Sugi has a relatively dense canopy cover structure.

The bare land class showed somewhat lower mean values of fractions in REM_{FE}, REM_{SE}, and REM_{LE} (0.008, 0, and 0.008, respectively), but a higher fraction in REM_{OE} (0.984) (Table 4). This result indictes that bare land did not provide multiple-returns. These data showed a distinct difference from other classes.

The description from the EIM

Among the EIMs with 3 classes of forest types, the EIM_{All}, EIM_{FE}, EIM_{SE}, EIM_{LE}, and EIM_{OE} showed higher intensity mean values for red cypress and Sugi than for mixed hardwoods (Table 5). Differences in mean values of intensity among red cypress, Sugi, and mixed hardwoods were supported by Schreier et al. (1985): the mean value of the laser intensity could be differentiated between coniferous and broadleaf trees. In this study, red cypress and Sugi are coniferous trees, while mixed hardwoods are broadleaf trees.

The EIM_{All}, EIM_{FE}, EIM_{SE}, EIM_{LE}, and EIM_{OE} showed higher-intensity DN values in red cypress than in Sugi. But the intensities of the DN values of those variables for red cypress were relatively closer to those of Sugi than to mixed hardwoods. This similarity may have been caused by the 2 forest types being coniferous trees, and their foliage shapes both being acerate.

In this study, vegetation classes showed higher-intensity DN values than bare land. The same finding was also reported by studies

Table 4. Descriptive statistics (mean and standard deviation) of the ratio of echo model (REM) for different land cover types

LiDAR-derived variable	Mean (standard deviation)			
	Red cypress	Sugi	Mixed hardwoods	Bare land
REM_{FE}	0.224 (0.055)	0.168 (0.032)	0.245 (0.061)	0.008 (0.014)
REM_{SE}	0.042 (0.021)	0.022 (0.010)	0.038 (0.020)	0 (0)
REM_{LE}	0.229 (0.060)	0.172 (0.039)	0.245 (0.064)	0.008 (0.014)
REM_{OE}	0.506 (0.125)	0.639 (0.071)	0.473 (0.135)	0.984 (0.028)

FE, first echo; SE, second echo; LE, last echo; OE, only echo.

Table 5. Descriptive statistics (mean and standard deviation) of the echo intensity model (EIM) for different land cover types

LiDAR-derived variable	Mean (standard deviation)			
	Red cypress	Sugi	Mixed hardwoods	Bare land
EIM_{All}	155.17(15.90)	149.21 (17.99)	122.68 (23.58)	71.47(56.32)
EIM_{FE}	149.95 (17.79)	95.87(20.47)	85.81 (22.24)	28.22 (39.10)
EIM_{SE}	65.78 (10.18)	43.84 (12.70)	46.11 (12.26)	3.92 (15.16)
EIM_{LE}	70.28(12.68)	60.63(16.41)	59.70 (11.77)	22.21 (29.45)
EIM_{OE}	199.28 (14.51)	187.46 (21.97)	174.50 (25.70)	66.63(59.92)

ALL, all echo types; FE, first echo; SE, second echo; LE, last echo; OE, only echo.

of Song et al. (2002) and Moffiet et al. (2005). Measurements of LiDAR intensity are sensitive to different ground textures, and can distinguish bare land from other vegetation classes.

Comparisons of echo types from LiDAR-derived variables

The vertical distribution of each echo type represents different vertical forest structures. The first echo is reflected from the canopy surface, the only echo from the canopy surface and canopy gap, the second echo from inside the canopy, and the last echo is reflected from the ground of forest land or inside the canopy (Fig. 2 right).

In order to give a brief outline of the collected data, Fig. 5 clearly shows DN value of the EIM and the fractional of value of the REM among 4 land cover types with different x-axis scales for each echo type. The value of REM_{OE} was much higher than those of the other echo types of the REM (Fig. 5 right) for all types. The higher proportion of only echoes was caused by high stand densities in the study area, in that the emitted laser light could not easily pass through the vegetation surface. Most of the only echoes were reflected from the canopy surface (Fig. 2 right). The REM_{OE} can be used to represent the canopy density, and the ratio of the only echo is related to the impermeability of the foliage cover (Moffiet et al. 2005). The REM_{OE} showed the highest fractional value in Sugi compared to red cypress and mixed hardwoods (Fig. 5 right). This means that Sugi had a higher foliage cover density. Otherwise, fractional values of the REM_{FE} and REM_{LE} were very similar among all vegetation types.

In intensity variables of all forest types, the EIM_{OE} showed a higher-intensity value than the other echo types with the EIM (Fig. 5 left), with the same outcome in Ørka et al. (2007)'s study. The higher-intensity value of the EIM_{OE} comes from the character of the only echo that provides a single return. The emitted light retains much higher energy in only echoes, so only echoes yielded higher-intensity DN values than the other echo types. The EIM_{FE} had the second intensity DN value in the EIM. The EIM_{SE}, and EIM_{LE} showed lower-intensity DN values in the EIM (Fig. 5 left). These results indicated that when the emitted laser light passed through the vegetation, the energy of the laser light decreased, which led to lower-intensity DN values in the multiple-return datasets. As the frequency of return increased and the intensity of the DN values decreased, the EIM_{SE} and EIM_{LE} produced lower DN values. The results described above fit the conditions of land-cover types in this study area.

Comparisons of LiDAR-derived variables among forest types

In this study, the researchers further tested LiDAR-derived variables for land cover classifications at the stand level. The transformed divergence (TD) was used to analyze the separability of the training data among these cover types. Results showed that TD values ranged 1870~2000; the separation was good, and all the classes could be separated (Table 6).

Duncan's test was also used to compare differences for the land types (Table 7). The EIM_{FE} and EIM_{OE} showed distinct differences in intensity mean values among the 3 forest types and bare land (Table 7). Ørka et al. (2007) also indicated that the intensity of the first echo was the most appropriate measure to discriminate tree species. However, there was some confusion between red cypress and Sugi in the EIM_{All}, and there was also some confusion between mixed hardwoods and Sugi in the EIM_{SE} and EIM_{LE} (Table 7).

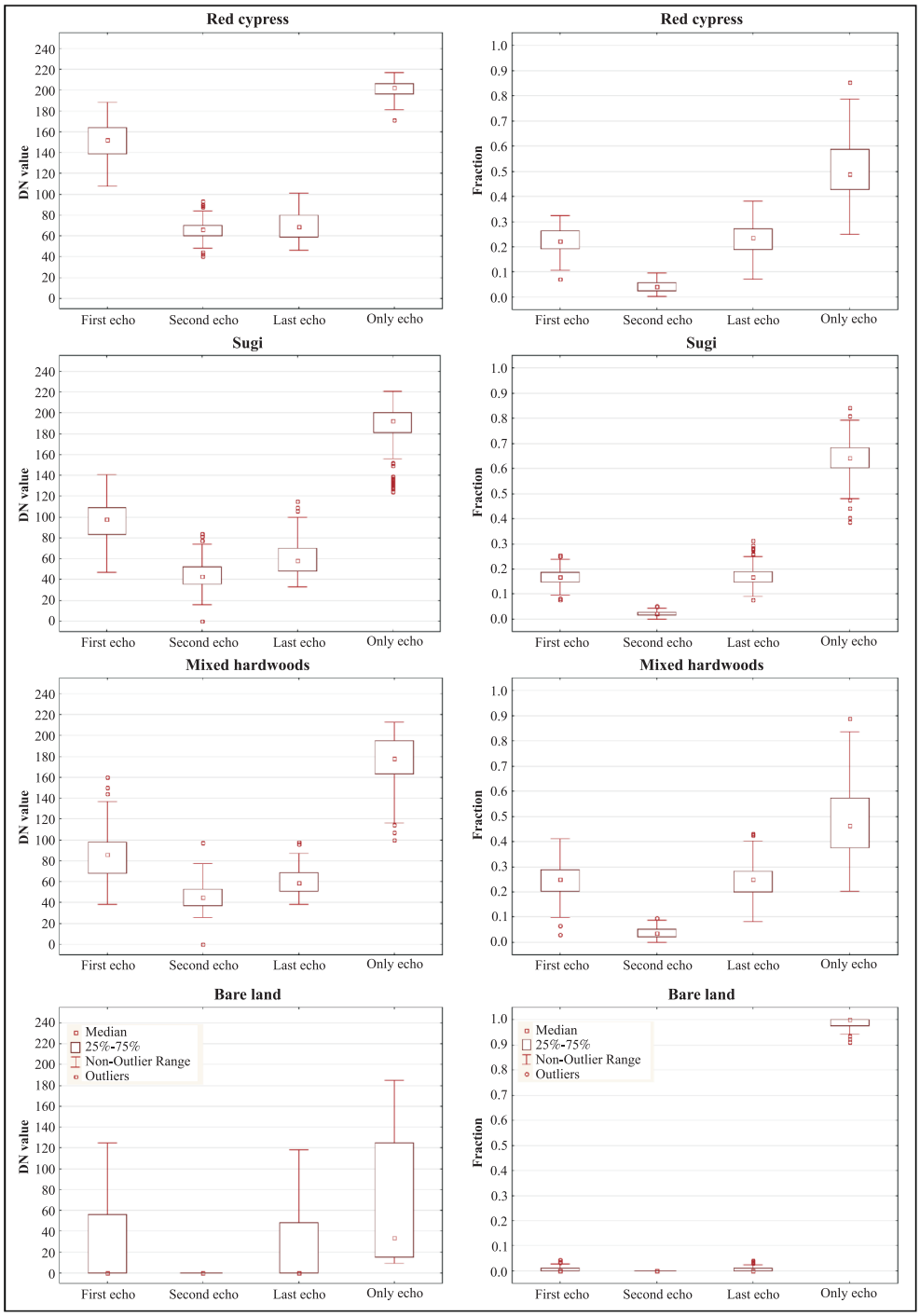

Fig. 5. Statistical distributions of the echo intensity model (EIM) and ratio of echo model (REM) in echo types for each forest cover type, (a) EIM of red cypress, (b) REM of red cypress, (c) EIM of Sugi, (d) REM of Sugi, (e) EIM of mixed hardwoods, (f) REM of mixed hardwoods, (g) EIM of bare land, (h) REM of bare land.

Table 6. Transformed divergence for training data

Class	Red cypress	Sugi	Mixed hardwoods
Red cypress			
Sugi	1998.13		
Mixed hardwoods	1944.01	1870.15	
Bare land	2000	2000	2000

All echo types of the REM showed distinct differences among land cover types (Table 7). In a study by Takahashi et al. (2006), the laser penetration rate differed between Hinoki cypress and Sugi stands, and a similar result was also found in this study as red cypress and Hinoki cypress are similar tree species. Results of this research also showed that all echo types of the REM could differentiate among Sugi, red cypress, and mixed hardwoods (Table 7). The canopy structure of Sugi and the other 2 forest types greatly differ, because Sugi has a smaller tree crown size (Fig. 2c). Thus, the result demonstrated that the REM can represent canopy density.

Actually, the REM can distinguish between Sugi and mixed hardwoods, and this result demonstrated that intensity data were also related to canopy density. Similarly as suggested by Schreier et al. (1985), LiDAR intensity provides exact information on the vegetation density. The REM_{FE}, $REM_{LE,}$ and REM_{OE} showed higher F values: 720.826, 610.271, and 692.788, respectively (Table 7). These values indicate that the REM_{FE}, REM_{LE}, and REM_{OE} had higher variations, and might carry more information about forest lands. In a study by Holmgren and Persson (2004), the proportions of first echoes outlined a high accuracy of classification for differentiating among tree species. Moffiet et al. (2005)'s research indicated that proportions of singular returns showed potential for assisting with species differentiation. The findings from those 2 studies also provide a fundamental basis for this study to develop. The first echo provided plenty of information for both the proportions of echo returns and the intensity data.

All echo types of the EIM and REM showed clear differences in the bare land class, because bare land did not provide multiple returns. So the EIM and REM can easily identify bare land from forest land.

Results of classification and accuracy assessments

LiDAR single image classification

The classification accuracies from the REM and EIM are displayed in Table 8,

Table 7. Results of Duncan's test

Images	*F*	Duncan's test			
EIM_{All}	211.079**	Bare land [a]	Mixed hardwoods [b]	Sugi [c]	Red cypress [c]
EIM_{FE}	434.459**	Bare land [a]	Mixed hardwoods [b]	Sugi [c]	Red cypress [d]
EIM_{SE}	461.419**	Bare land [a]	Mixed hardwoods [b]	Sugi [b]	Red cypress [c]
EIM_{LE}	163.451**	Bare land [a]	Mixed hardwoods [b]	Sugi [b]	Red cypress [c]
EIM_{OE}	437.435**	Bare land [a]	Mixed hardwoods [b]	Sugi [c]	Red cypress [d]
REM_{FE}	720.826**	Bare land [a]	Sugi [b]	Red cypress [c]	Mixed hardwoods [d]
REM_{SE}	191.905**	Bare land [a]	Sugi [b]	Mixed hardwoods [c]	Red cypress [d]
REM_{LE}	610.271**	Bare land [a]	Sugi [b]	Mixed hardwoods [c]	Red cypress [d]
REM_{OE}	692.788**	Red cypress [a]	Mixed hardwoods [b]	Sugi [c]	Bare land [d]

Land types in a row followed by the same letter do not significantly differ.
ALL, all echo types; FE, first echo; SE, second echo; LE, last echo; OE, only echo.

Table 8. Classification accuracy of single images

	Overall classification accuracy (%)	Overall Kappa statistics
EIM_{All}	53.5	0.39
EIM_{FE}	68.0	0.57
EIM_{SE}	60.0	0.47
EIM_{LE}	50.5	0.34
EIM_{OE}	52.0	0.37
REM_{FE}	68.5	0.58
REM_{SE}	51.5	0.36
REM_{LE}	66.0	0.55
REM_{OE}	66.5	0.55

ALL, all echo types; FE, first echo; SE, second echo; LE, last echo; OE, only echo.

where the highest classification accuracy of overall classification was with the REM_{FE}, at 68.5% (Table 8). This result matched the finding of Holmgren and Persson (2004), where a higher classification accuracy, using a discrimination analysis with the proportion of first echoes, reached 78.0%.

The overall classification accuracy of the REM_{OE} was 66.5% (Table 8). Moffiet et al. (2005) also noted that the proportion of only echoes can potentially discriminate species. In Holmgren and Persson (2004)'s paper, the higher overall classification accuracy, with proportion of surface returns, was 75.6%. In this study with a higher classification accuracy, most of the only echoes were reflected on the canopy surface, so only echoes could represent the surface return.

Classification results from the EIM_{FE} showed a higher classification accuracy of intensity data of up to 68.0% (Table 8). Ørka et al. (2007) applied a linear discriminant analysis (LDA) to analyze the mean intensity of first echoes for classifying tree species at the single tree level, and they achieved the highest overall accuracy of up to 68.3%. Ørka et al. (2007) also indicated that the intensity of first echoes was the most appropriate measure for separating tree species, with the same results as in our research.

Results of the single image classification indicated that LiDAR-derived variables have the capability to classify forest types; and all variables showed a range of classification accuracies of 50.5~68.5% (Table 8). Generally speaking, the EIM_{FE}, REM_{FE}, REM_{LE}, and REM_{OE} had higher potential for forest type classification, but for more-accurate mapping results, the overall classification accuracy was still low. Each variable may possess different information from the 4 land types, and the variable may have been complementarily characterized**.** Thus, combining those variables may produce more-precise results for accuracy.

LiDAR stack image classification

This study found that if LiDAR-derived variables for image classification were combined with those variables, there would be more-precise results for accuracy. For LiDAR stack image classification, the highest accuracy of the overall classification reached 81.5%, with overall Kappa statistics of 0.75 (Table 9). According to the accuracy of the producer, red cypress and bare land had higher accuracy producers, at 89.2 and 88.7, respectively (Table 9). It is not difficult to see the misclassification of Sugi and mixed hardwoods which contained most of the errors. The composition of mixed hardwoods was complex, and this may have caused most of the errors. However, the result was still good and acceptable. The final map of classification is shown in Fig. 6.

Stacking all of the data for classification processing may result in complex information, and the results showed that stacked images carried more-complete information, and greatly increased the classification accuracy. The results proved that the classification

accuracy was higher than with single image classification processing at up to 81.5%. In Holmgren and Persson (2004)'s paper, the higher classification accuracy reached 95%, by combining 6 LiDAR-derived variables. Bartels and Wei (2006)'s study indicated that combining more LiDAR-derived variables would achieve higher classification results.

Table 9. Error matrix resulting from LiDAR stack images

Class name	RC	SG	MH	BL	Total	User's accuracy (%)
Red cypress (RC)	**33**	03	06	03	045	73.3
Sugi (SG)	02	**36**	08	03	049	73.5
Mixed hardwoods (MH)	02	09	**47**	-	058	81
Bare land (BL)	-	-	01	**47**	048	97.9
Total	37	48	62	53	200	-
Producer's accuracy (%)	89.2	75	75.8	88.7	-	-
Overall accuracy	**81.5%**					
Overall Kappa statistics	**0.75**					

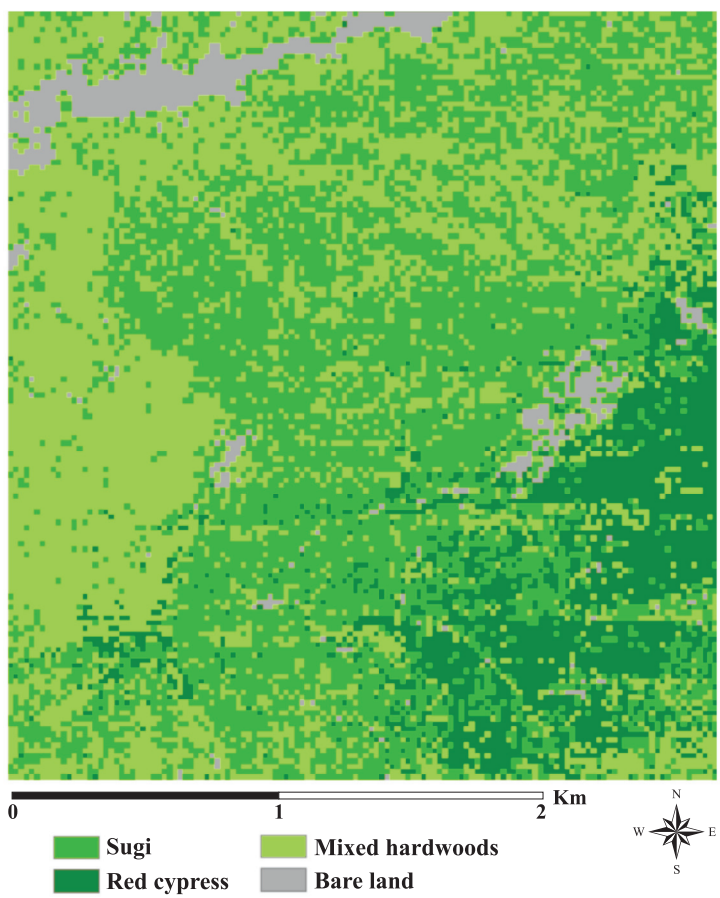

Fig. 6. Forest cover map based on LiDAR stack image classification.

Ørka et al. (2007) believed that combining more LiDAR-derived variables produced a higher accuracy and probably improved the classification results, with the highest classification accuracy up to 73.2%, when combining all of the intensity variables. The results of stack image classification indicated that combining LiDAR-derived variables can be used to generate accurate forest type maps.

CONCLUSIONS

Results of this study indicate that LiDAR multiple-return and intensity data can be used for classifying land cover types. In this research, the REM and EIM were effective in identifying differences in forest types. The LiDAR intensity also provided information on the density of the vegetation. When the emitted laser light passed through the vegetation, the energy of the laser light decreased, leading to lower-intensity DN values for the EIM_{SE} and EIM_{LE}. In the evaluation of echo types, the first echo produced plentiful information in both the proportions of echo returns and intensity data. LiDAR multiple-return characters were useful in identifying bare land, because bare land did not produce multiple returns. In the intensity data, bare land provided a lower-intensity DN value that can be useful in easily identifying bare land.

Results of the single image classification pointed out that LiDAR-derived variables have the capability to classify forest types. Generally speaking, the EIM_{FE}, REM_{FE}, REM_{LE}, and REM_{OE} showed higher potential for forest-type classification. Results of stack image classification indicated that combining more LiDAR-derived variables generated more-accurate forest type maps, and this procedure obtained the highest overall classification accuracy of up to 81.5%. In the near future, integrating LiDAR data and other data of optical remote sensing will become an outstanding advancement in the field of forest mapping.

ACKNOWLEDGEMENTS

The authors would like to thank the Energy and Resources Laboratories of the Industrial Technology Research Institute (Hsinchu, Taiwan) for providing data for this study.

LITERATURE CITED

Bartels M, Wei H. 2006. Maximum likelihood classification of LiDAR data incorporating multiple co-registered bands. Fourth International Workshop on Pattern Recognition in Remote Sensing in conjunction with the 18th International Conference on Pattern Recognition 2006, Hong Kong. p 17-20.

Donoghue DNM, Watt PJ, Cox NJ, Wilson J. 2007. Remote sensing of species mixtures in conifer plantations using LiDAR height and intensity data. Remote Sens Environ 110:509-22.

Höfle B, Geist T, Rutzinger M, Pfeifer N. 2007. Glacier surface segmentation using airborne laser scanning point cloud and intensity data. ISPRS Workshop on Laser Scanning 2007 and SilviLaser 2007, Espoo, 12-14 September 2007, Finland. p 195-200.

Holmgren J, Persson Å. 2004. Identifying species of individual trees using airborne laser scanner. Remote Sens Environ 90:415-23.

Jensen JR. 1996. Introductory digital image processing: a remote sensing perspective. 2nd edition. Englewood Cliffs, NJ: Prentice-Hall.

Lefsky MA, Cohen WB, Acker SA, Parker GG, Spies TA, Harding D. 1999. LiDAR remote sensing of the canopy structure and biophysical properties of Douglas-fir western hemlock forests. Remote Sens Environ 70(3):339-61.

Lefsky MA, Cohen WB, Parker GG, Harding DJ. 2002. LiDAR remote sensing for ecosystem studies. Bioscience 52:19-30.

Maltamo M, Eerikäinen K, Pitkänen J, Hyyppä J, Vehmas M. 2004. Estimation of timber volume and stem density based on scanning laser altimetry and expected tree size distribution functions. Remote Sens Environ 90:319-330.

Means J, Acker S, Fitt B, Renslow M, Emerson L, Hendrix C. 2000. Predicting forest stand characteristics with airborne laser scanning LiDAR. Photogramm Engin and Remote Sens 66(11):1367-71.

Moffiet T, Mengersen K, Witte C, King R, Denham R. 2005. Airborne laser scanning: Exploratory data analysis indicates potential variables for classification of individual trees of forest stands according to species. ISPRS J Photogramm 59:289-309.

Morsdorf F, Kötz B, Meier E, Itten KI, Allgöwer B. 2006. Estimation of LAI and fractional cover from small footprint airborne laser scanning data based on gap fraction. Remote Sens Environ 104:50-61.

Næsset E. 1997a. Determination of mean tree height of forest stands using airborne laser scanner data. ISPRS J Photogramm 52(2):49-56.

Næsset E. 1997b. Estimating timber volume of forest stands using airborne laser scanner data. Remote Sens Environ 61(2):246-53.

Næsset E. 2002. Predicting forest stand characteristics with airborne scanning laser using a practical two-stage procedure and field data. Remote Sens Environ 80:88-99.

Nilsson M. 1996. Estimation of tree heights and stand volume using an airborne LiDAR system. Remote Sens Environ 56(1):1-7.

Ørka HO, Næsset E, Bollandsås OM. 2007. Utilizing airborne laser intensity for tree species classification. International Society for Photogrammetry and Remote Sensing Workshop on Laser Scanning 2007 and SilviLaser 2007, Espoo, 12-14 September 2007, Finland. p 300-4.

Peng BS, Hsieh YT, Chen CT. 2008. Relationship between the airborne laser penetration index and leaf area index by LiDAR data analysis of a Sugi plantation. Taiwan J For Sci 23(Suppl):S63-73.

Raymond M. 1992. Measures laser remote sensing: fundamentals and applications. Malabar, FL, Krieger Publishing. p 510.

Schreier H, Lougheed J, Tucker C, Leckie D. 1985. Automated measurements of terrain reflection and height variations using an airborne infrared laser system. Int J Remote Sens 6(1):101-13.

Song J, Han S, Yu K, Kim Y. 2002. Assessing the possibility of landcover classification using LiDAR intensity data. Graz, Austria: International Society for Photogrammetry and Remote Sensing Commission III. p 9-13.

Suarez JC, Ontiveros C, Smith S, Snape S. 2005. Use of airborne LiDAR and aerial photography in the estimation of individual tree heights in forestry. Comput Geosci 31:253-62.

Takahashi T, Yamamoto K, Miyachi Y, Senda Y, Tsuzuku M. 2006. The penetration rate of laser pulses transmitted from a small-footprint airborne LiDAR: a case study in closed canopy, middle-aged pure Sugi (*Cryptomeria japonica* D. Don) and Hinoki cypress (*Chamaecyparis obtusa* Sieb. et Zucc.) stands in Japan. J For Res-Jpn 11:117-23.

Wehr A, Lohr U. 1999. Airborne laser scanning - an introduction and overview. ISPRS J Photogramm 54(2-3):68-82.

Zimble DA, Evans DL, Carison GC, Parker RC, Grado SC, Gerard PD. 2003. Characterizing vertical forest structure using small-footprint airborne LiDAR. Remote Sens Environ 87(2, 3):171-82.